Kinetic modelling studies of heterogeneously catalyzed biodiesel synthesis reactions

Ankur Kapil[†], Karen Wilson[††], Adam F Lee[††], Jhuma Sadhukhan[†]*

[†]Centre for Process Integration, School of Chemical Engineering and Analytical Science, The University of Manchester, Manchester, M13 9PL, UK

[††]Cardiff School of Chemistry, Cardiff University, Main Building, Park Place, Cardiff, CF10 3AT

[*]Author to whom correspondence should be addressed
E-mail: jhuma.sadhukhan@manchester.ac.uk
Phone : +44-161-3064396
Fax: +44 -161-236 7439

Abstract

The heterogeneously catalysed transesterification reaction for the production of biodiesel from Triglycerides was investigated for reaction mechanism and kinetic constants. Three elementary reaction mechanisms Eley-Rideal (ER), Langmuir–Hinshelwood–Hougen–Watson (LHHW), and Hattori with assumptions such as quasi steady state conditions for the surface species and methanol adsorption, and surface reactions as the rate determining steps were applied to predict the catalyst surface coverage and the bulk concentration using a multi-scale simulation framework. The rate expression based on methanol adsorption as the rate limiting in LHHW elementary mechanism has been found to be statistically the most reliable representation of the experimental data using hydrotalcite catalyst with different formulations.

Keywords: Biodiesel, transesterification, heterogeneous catalysts, elementary reaction kinetics, hydrotalcites

1 Introduction

Biodiesel is a state-of-the-art renewable fuel produced by reacting vegetable oils, refined oils and animal fats, containing triglycerides and free fatty acids as the main constituents, with methanol[1]. The three main reactions steps in transesterification of Triglyceride with methanol are given in Equations 1-3[2]. In these reactions, Triglyceride (*T*), Diglyceride (*D*), and Monoglyceride (*M)* react with methanol (CH_3OH) to form *D*, *M* and glycerol (*G*) respectively along with Methyl Oleate (*MeOl*), or longer chained methyl ester - depending on glyceride chain length.

$$T + CH_3OH \Leftrightarrow D + MeOl \quad \textbf{1}$$

$$D + CH_3OH \Leftrightarrow M + MeOl \quad \textbf{2}$$

$$M + CH_3OH \Leftrightarrow G + MeOl \quad \textbf{3}$$

Heterogeneously catalysed transesterification reactions[3, 4] that include alkali oxides[5, 6], alkaline earth oxides[7-9], zeolites[10, 11], and hydrotalcites[12-15], are preferred over homogeneous reactions, due to various reasons, including soap formation, catalyst loss and involvement of significantly more number of separation steps in the latter case. Dossin et al.[2, 16] introduced the kinetic studies of MgO catalyzed transesterification of alkyl esters with methanol using ER type mechanism. Their model is based on the following assumptions: i) adsorption of methanol as the rate

determining step; ii) all other reactions assumed to be in equilibrium, and iii) equal rate constants for the forward reaction in all the three basic reactions steps (Equations 1-3). They developed a kinetic model based on a single elementary reaction mechanism with assumption of methanol adsorption as rate limiting step, for a single composition of MgO catalyst. Building on their work, the scope of this work was to undertake comprehensive kinetic studies of heterogeneously catalyzed transesterification reactions. Three mechanistic kinetic models, ER (considering reaction of triglyceride with adsorbed methanol), LHHW (considering adsorption of triglyceride on the catalyst surface) and Hattori (considering formation of intermediates from every elementary reaction step), with various assumptions on rate determining steps and quasi steady state for surface species have been analysed. The experimental results presented in Appendix A are based upon hydrotalcites catalysts with four different formulations $Mg_{0.81}Al$, $Mg_{1.38}Al$, $Mg_{1.82}Al$, and $Mg_{2.93}Al$, referred as MG1, MG2, MG3, and MG4, respectively[14]. These catalysts are micro-porous with active sites concentrated on their surface, reducing the requirement for bulky glyceride species diffusing through micro-pores, whilst providing rigidity through the layered structure.

The hierarchical modelling of reactions is essential to evaluate the effect of micro scale surface evolution on the changes in bulk concentration and vice versa and thereby validate reaction mechanisms[17]. Karpov et al.[18] considered the coupling of Monte Carlo with the continuum finite element method (FEM) equations for fuel cell catalysts and binary material systems applications. Levchenko et al.[19] used multiscale Monte Carlo/ surface diffusion numerical equation to study the growth of metal catalyst particles by deposition from a low-temperature plasma. Majumder et al.[20] developed a multiscale modelling approach combining Monte Carlo simulations with finite difference solver. They established their method by comparison with a continuum method. The methodology was applied to two reaction mechanism for unimolecular and bimolecular reactions. Vlachos et al.[21] applied a hierarchical multiscale simulation framework for model-based design of experiments. The multiscale model was applied to two case studies for ammonia decomposition on ruthenium to produce hydrogen and the water-gas shift reactions on platinum for converting syngas to hydrogen. Raimondeau et al.[22] applied multiscale simulations to study the effect of species spatial inhomogeneity to the catalytic oxidation of CO on Pt. By adapting these modelling tools and insights, this work aims to integrate catalytic surface kinetic Monte Carlo (KMC)[23] and bulk scale mean field (MF) simulations[24] in order to validate the kinetic

parameters estimated using genetic algorithm (GA) based optimisation approach[25, 26]. The kinetic parameters obtained correspond to the appropriate match between simulation and experimental results of evolution in bulk concentrations.

The overall modelling strategy is discussed in the next section. Estimation of kinetic rate constants using GA based optimization methodology, followed by their validation using multi-scale KMC/MF simulation framework is outlined. Thereafter, ER, LHHW, and Hattori mechanisms alongside the derivations of the kinetic rate expressions are illustrated. The results of various mechanisms are quantitatively analysed and compared for the selection of the most appropriate mechanism that may be valid for the whole range of formulations. Simultaneously, the analysis may also suggest the best mechanism for individual formulations.

2 Methodology

The overall strategy for an estimation of kinetic rate constants based on a reaction mechanism is illustrated as follows (Figure 1).

1. The rate parameters involved in an assumed mechanism were estimated using GA based optimisation.
2. Using the rate constants obtained from step 1, the distribution of species on the surface of a catalyst formulation as well as the changes in bulk specie concentrations were predicted by a multi-scale KMC/MF simulation framework implemented. This framework was used to simultaneously capture the effect of surface adsorption-reaction-desorption on the bulk specie concentrations. An iteration of rate constants between the GA based optimisation step and the multi-scale KMC/MF simulation step may be involved, until the best fit of concentration profiles against experimental results is obtained.
3. The mechanism is applied to various catalyst formulations.
4. New mechanisms and assumptions were then considered for the parametric prediction using the above two frameworks, GA based optimisation and multi-scale KMC/MF simulation, until all three mechanisms with given assumptions are investigated.
5. Statistical reliance and comparison between mechanisms were performed. This analysis may propose the most appropriate mechanism that may be valid for the whole range of formulations or suggest the best mechanism for individual formulations.

Figure 1: Overall strategy to investigate into reaction mechanisms

Determination of kinetic rate constants using GA

The steps for the estimation of the rate constants by applying GA based optimization are as follows.

1. The initial concentrations in the batch reactor ($C_i(0)$), size of the reactor, and batch time are specified (Appendix A). The bounds for the rate constants k_j are also provided as the inputs to the GA (Appendix B).
2. The rate constants are decision variables and their initial values are guessed by GA using random number generator in between their respective bounds.
3. The bulk concentration (C_i) of specie *i* is a function of kinetic rates (R_i), Equation 4.

$$\frac{dC_i}{dt} = R_i \qquad \forall i \in T, D, M, G, MeOl, CH_3OH \qquad (4)$$

4. To account for the non-ideality of a mixture as in here, the correlation between the activity of specie ($[i]$) and its concentration C_i in Equation 5 was applied. The UNIFAC contribution method[27] outlined in Appendix C was used to calculate the activity coefficients, γ_i. Table 1 exemplifies typical values of activity coefficients of species.

$$[i] = C_i \gamma_i \qquad \forall i \in T, D, M, G, MeOl, CH_3OH \qquad (5)$$

5. The set of ordinary differential equations (Equation 4) was solved by ode45 solver in MATLAB with a time gap of 1s. The bulk concentrations profiles of species in the reactor is obtained as a function of time.
6. The GA optimization, based on the works of Bhat et al.[25] and Xu et al.[26], [28], implemented in MATLAB (Appendix B) was then applied to minimise the residual sum of square (*RSSQ*) of errors between the experimentally observed and the model predicted concentrations of species (*i* = 1 to *nspc*), at subsequent time points (*j* = 1 to *ntime*), in Equation 6, by adjusting the rate constants within their specified ranges. It is assumed that the rate of reaction for adsorption of methanol is a low value in the range of 10^{-1} while that for other reaction rate constants are in 2 orders of magnitude.

$$RSSQ = \sum_{j=1}^{ntime} \sum_{i=1}^{nspc} \left(C_i(j) - C_i^{epxerimental}(j) \right)^2 \qquad (6)$$

7. GA generates new sets of rate constants. *RSSQ* is re-evaluated according to Equation 6.
8. Simulations were repeated until *RSSQ* is <0.005 or the number of iterations exceeds the maximum (100000).

Table 1: Activity coefficients of species

Multi-scale KMC/MF simulation framework

Once the preliminary rate constants were estimated by GA based optimisation, these parameters were further verified using a multi-scale KMC/MF simulation framework implemented in MATLAB (Figure 2).

1. The concentrations of species on the surface of the catalyst, and the concentrations in the bulk were the inputs to the KMC algorithm. The surface of the catalyst was considered to be empty at the start of a reactor run. The initial bulk concentrations were obtained from the work of Cantrell et al.[14](Appendix A).
2. The surface concentration was assumed to be constant during mean field simulation over a small time interval *dt*(~1s). The bulk concentration changes were updated by the mean field simulation of the ordinary differential equation in the bulk phase (Equation 4). The rate of change of concentration was defined on the basis of kinetic rates in the elementary reaction mechanism.
3. Similarly, the bulk concentration was assumed to be constant over a small time interval *dt*, during which the KMC simulation on the catalyst surface was undertaken. The KMC simulation relied upon the event probability based on their respective rate constants. The surface concentration is advanced in time by KMC simulation[23].
4. The overall time is advanced as the times for KMC and MF simulations are updated.
5. The simulation is continued for the total run time of a reactor (in this case 10800s, Appendix A).

Figure 2: Multi-scale KMC/MF simulation framework

Three elementary reaction mechanisms, ER, LHHW and Hattori, along with the rate expressions depending upon the assumptions on the rate determining steps and quasi steady states, are discussed next.

ER mechanism

The elementary reactions in ER kinetic mechanism are shown in Table 2. The mechanism involves adsorption of methanol on empty catalyst sites and reactions between adsorbed methanol (CH_3OH^*) with T, D and M in the bulk to form adsorbed diglyceride (D^*), monoglyceride (M^*) and glycerol (G^*) respectively along with methyl oleate ($MeOl$).

Table 2: Elementary reactions in ER mechanism

Each of these steps can be treated as a rate determining step. The surface of the catalyst was assumed to be homogeneous without any inert specie in all cases. The rates of generation and consumption of bulk species in Table 2 were derived based on the assumption of quasi steady state conditions of the surface species, in Table 3. Hence, the concentrations of the catalyst surface species remained constant with respect to time. Additionally, the backward reaction rate constants were neglected. k_1-k_7 in Table 3 represent the kinetic rate constants of the forward reactions in 7 elementary steps in Table 2. $[D],[T],[M],[G],[CH_3OH],[MeOl]$ are the activities of diglyceride, triglyceride, monoglyceride, glycerol, methanol and methyl oleate respectively in the bulk phase.

Table 3: Kinetic reaction rate expressions for ER quasi steady state mechanism

LHHW mechanism

The elementary reactions in LHHW kinetic mechanism are given in Table 4. The first step is the adsorption of methanol. The main difference between ER and LHHW mechanism is the adsorption of triglyceride on the surface of the catalyst. The adsorbed methanol and triglyceride react with each other if they are adjacent, to produce adsorbed diglyceride and methyl oleate respectively. Subsequently this adsorbed methanol reacts with adsorbed diglyceride or monoglyceride to form adsorbed monoglyceride, and glycerol respectively along with methyl

oleate. Table 4 presents the expressions for equilibrium rate constants K_1-K_9, for the 9 elementary reaction steps in LHHW mechanisms respectively.

Table 4: Elementary reactions in LHHW mechanism

In addition to the adsorbed species defined in ER mechanism * and *T** were introduced to represent empty site and adsorbed triglyceride on the catalyst surface, respectively. k_j indicates the forward reaction kinetic rate constants for the 9 rate determining steps, and K_j represents the equilibrium constants of reaction *j*, respectively, in Table 4. The elementary reaction expressions in Table 4 lead to the kinetic rate expressions for individual reaction steps, in Table 5.

Table 5: Elementary reaction rate expressions for LHHW mechanism with surface reaction as rate limiting

Hattori mechanism

The elementary reactions in Hattori kinetic mechanism are provided in Table 6. Similar to LHHW, Hattori mechanism also considers the adsorption of triglyceride on the surface of the catalyst as a rate determining step. Hattori mechanism differs from LHHW mechanism, where in the formation of intermediate species from the reactions between adsorbed methanol and adsorbed triglyceride, diglyceride and monoglyceride is considered. The adsorbed methanol and triglyceride react to form adsorbed intermediate ($TsCH_3OH$*) and an empty site respectively. Subsequently, the adsorbed intermediate ($TsCH_3OH$*) decomposes into the production of adsorbed diglyceride and bulk methyl oleate respectively. Adsorbed diglyceride, monoglyceride and glycerol thereafter desorb from the catalyst surface into the bulk phase. $TsCH_3OH$*, $DsCH_3OH$*, $MsCH_3OH$* represent the intermediates from the reactions between adsorbed methanol and adsorbed *T*, *D* and *M* respectively. The elementary reaction expressions in Table 6 result in the kinetic rate expressions in Table 7.

Table 6: Elementary reactions in Hattori mechanism

Table 7: Elementary reaction rate expressions for Hattori mechanism with methanol adsorption as rate limiting

k_j indicates the forward reaction kinetic rate constants for 11 rate determining steps, and K_j represents the equilibrium constant of reaction *j*, respectively, in Table 6.

3 Results and discussions

The GA optimisation (Appendix B) and KMC/MF simulation (Figure 2) frameworks were implemented in a PC with Pentium® D CPU 3.00 GHz processor and 1GB RAM. The run time for the convergence of one mechanism applied to a catalyst formulation is 105 minutes. Five kinetic models based on the three elementary reaction mechanisms, ER (Table 2), LHHW (Table 4) and Hattori (Table 7) with assumptions on quasi steady state of surface species and methanol adsorption and surface reaction as rate limiting steps were investigated, as follows.

- ER quasi steady state
- ER methanol adsorption as rate determining
- LHHW surface reaction as rate limiting
- LHHW methanol adsorption as rate limiting
- Hattori methanol adsorption as rate determining

The statistical significance of a mechanism is achieved by Chi square χ^2 test. The results of kinetic parameters and chi square test for statistical significance are presented in Table 8. It is calculated as the ratio of the residual sum of the square of the errors (RSSQ) between the predicted and the experimental values for the concentrations of the species (i = 1 to *nspc*), at time points (j = 1 to *ntime*) and the experimental values at given data points, in Equation 7 [28].

$$\chi^2 = \sum_{j=1}^{ntime} \sum_{i=1}^{nspc} \frac{\left(C_i(j) - C_i^{epxerimental}(j)\right)^2}{C_i^{epxerimental}(j)} \qquad 7$$

Table 8: Prediction of kinetic rate constants and χ^2 for different mechanisms and catalysts

The simulation results of ER quasi steady state mechanism (Table 3) on $Mg_{2.93}Al$ hydrotalcite catalyst are illustrated in detail, while other system results are only summarised.

Results of application of ER quasi steady state mechanism to hydrotalcite catalyst $Mg_{2.93}Al$

The results of kinetic parameters ($k_{1\text{-}7}$) in ER quasi steady state mechanism (Table 3) on $Mg_{2.93}Al$ hydrotalcite catalyst using GA and multi-scale KMC/MF simulation framework are provided in Figure 3, Figure 4, and Figure 5 respectively. The RSSQ resulted (0.008) is higher than the specified for GA optimisation. However, the χ^2 value of 0.0044 in Table 8 is smaller than 0.01 required for 99.5% level of significance (confidence) with 7 degrees of freedom, in chi square test for statistical significance[29], implying higher level of significance / applicability of the mechanism.

Figure 3: Comparison between (a) fractional conversion of Triglyceride (T); (b) moles of Diglyceride (D); and (c) moles of Monoglyceride (M); for $Mg_{2.93}Al$ hydrotalcites obtained from ER quasi steady state model

The multi-scale simulation framework results into the time evolution of surface species, based on which the quasi steady hypothesis assumed at the first place can be validated. The results of the KMC/MF simulation presented in Figure 4 indicate a rapid initial change in the concentration of the species on the surface. However, subsequently steady state surface coverage fraction of 0.05 and 0.0003 were attained by the adsorbed species M* and CH_3OH*, respectively, after 1000s, while D* and G* eventually reached to their steady states at 0.09 and 0.84 respectively, after 10,000s (Figure 4). Hence, a steady state equilibrium attained by surface species reinforces the assumption on their quasi steady state.

Figure 4: Time evolution of surface species from KMC simulation

Figure 5 shows the evolution of catalyst surface resulted from KMC simulations. Initially the catalyst surface lattice is made up of empty sites (.) (Figure 5 case (a)). These lattice sites are converted into adsorbed methanol (~). However, the reaction of methanol with high concentration of triglyceride in bulk phase is fast. Hence most of the adsorbed methanol is converted into adsorbed diglyceride (+), 97.1% in case (b) Figure 5. A fraction of the adsorbed diglyceride is subsequently converted into adsorbed monoglyceride (ω) and finally into glycerol (°), 25.3% of each in case (c) Figure 5 over the duration of the reaction (10800s).

Figure 5: Evolution of catalyst surface from KMC simulations; *(.), CH_3OH*(~), D*(+), M*(ω), G*(º). Case (a) * (100%), CH_3OH*(0), D*(0), M*(0), G*(0) at t=0s; Case (b) * (2.9%), CH_3OH*(0.07%), D*(97.1%), M*(0), G*(0) at t=2000s ; Case (c) * (5.4%), CH_3OH*(0.1%), D*(43.9%), M*(25.3%), G*(25.3%) at t=10800s;

The kinetic parameters (Table 8) thus obtained by following the strategy in Figure 1 for ER quasi steady state reaction mechanism represents the experimental observation for $M_{2.93}Al$ hydrotalcite catalyst adequately. These frameworks were further applied to the other hydrotalcite catalysts with different concentrations of Mg and Al (Appendix A).

Results of application of ER quasi steady state mechanism for all hydrotalcite catalysts

The RSSQ and χ^2 obtained for $Mg_{1.82}Al$ hydrotalcite catalyst are 0.006 and 0.0218, respectively, indicating statistically good representation of the experimental data for $Mg_{1.82}Al$ hydrotalcite catalyst. Table 8 demonstrates statistically acceptable χ^2 values of 0.0174, 0.0218, and 0.0044 for the hydrotalcite catalysts, $Mg_{0.82}Al$, $Mg_{1.82}Al$, and $Mg_{2.93}Al$, respectively. However, the results for $Mg_{1.38}Al$ indicate a higher value of χ^2 (0.2611), revealing inconsistency in predicting the ER quasi steady state model for all four catalysts.

ER elementary reaction mechanism (Methanol adsorption as rate limiting)

From the illustration earlier, it was rational to assume methanol adsorption as a rate determining step in the ER mechanism. The resulting mechanism was further simplified by the assumption of equal rate constants of all the adsorption equilibrium steps, based on the work of Dossin et al.[2]. The equilibrium constant for the adsorption of methanol (K_{eq}) was assumed to be constant and equal to unity. The kinetic rate expression was reduced to two parameters k_f (rate of forward reaction for adsorption of methanol), and K_A (adsorption equilibrium constant for diglyceride, monoglyceride, glycerol and methyl oleate) (Equations 8, 9, and 10). Table 8 illustrates the χ^2 of 0.028, 0.03, 0.1722 and 0.013 for $Mg_{0.82}Al$, $Mg_{1.38}Al$, $Mg_{1.82}Al$, and $Mg_{2.93}Al$, respectively which is much less than 1.72 required for individual catalysts for the two parameter kinetic model with 9 degrees of freedom at 99.5% level of fit[29]. The degree of freedom is the number of experimental points (12) – the number of kinetic parameters (2) -1. Hence the kinetic model based on ER mechanism with methanol adsorption as rate limiting, can be applied to all four

hydrotalcite catalysts. The χ^2 value certainly improves for $Mg_{1.38}Al$ case from the quasi steady state assumption.

$$r_T = \frac{k_f\left([CH_3OH] - \frac{1}{K_{eq}}\frac{[D][MeOl]}{[T]}\right)}{\left(1 + \frac{K_A}{K_{eq}}\frac{[D][MeOl]}{[T]} + K_A[MeOl] + K_A[T] + K_A[D] + K_A[M] + K_A[G]\right)} \quad (8)$$

$$r_D = \frac{k_f\left([CH_3OH] - \frac{1}{K_{eq}}\frac{[M][MeOl]}{[D]}\right)}{\left(1 + \frac{K_A}{K_{eq}}\frac{[M][MeOl]}{[D]} + K_A[MeOl] + K_A[T] + K_A[D] + K_A[M] + K_A[G]\right)} \quad (9)$$

$$r_M = \frac{k_f\left([CH_3OH] - \frac{1}{K_{eq}}\frac{[G][MeOl]}{[M]}\right)}{\left(1 + \frac{K_A}{K_{eq}}\frac{[G][MeOl]}{[M]} + K_A[MeOl] + K_A[T] + K_A[D] + K_A[M] + K_A[G]\right)} \quad (10)$$

The lowest rate constant corresponds to methanol adsorption (k_f) with values of 1.6×10^{-6}, 1.71×10^{-6}, 7.33×10^{-6} and 7.12×10^{-6} for the four hydrotalcite catalysts, with increasing Mg concentration, respectively, revalidating the assumption (Table 8). However, ER mechanism assumes no adsorption for triglyceride, diglyceride, and monoglyceride in the bulk to react with adsorbed methanol. Triglyceride, diglyceride, and monoglyceride are large molecules and therefore their adsorption onto the catalyst surface would be difficult and hence can be regarded as rate determining steps, such as in LHHW and Hattori mechanisms discussed as follows.

LHHW elementary reaction mechanism (Surface reaction as rate limiting)

The kinetic rate constants for LHHW mechanism comprising of elementary steps in Table 4 are shown in Table 8. As can be seen from the results, the equilibrium reaction rate constant between adsorbed methanol and adsorbed diglyceride (K_4), is the fastest with the values of 0.37, 0.48 and 0.44 for $Mg_{0.81}Al$, $Mg_{1.38}Al$ and $Mg_{2.93}Al$ respectively (in the case of $Mg_{1.82}Al$ reaction between adsorbed methanol and adsorbed triglyceride (K_3) is found to be the fastest with a value of 0.15). It is consistently identified that K_1, the equilibrium constant of adsorption of methanol is the

slowest with 5.97×10^{-5}, 0.0001, 3.3×10^{-5} and 0.0001 for all four hydrotalcite catalysts, respectively (Table 8). χ^2 of 0.0061, 0.0203, 0.0092, and 0.0129 are predicted for $Mg_{0.81}Al$, $Mg_{1.38}Al$, $Mg_{1.82}Al$, and $Mg_{2.93}Al$, respectively, which are larger than 0.00 required for ten parameter kinetic model with 1 degree of freedom at 99.5% level of fit[29]. Hence the kinetic model based on LHHW surface reaction rate limiting cannot be applied to any of the four hydrotalcite catalysts at 99.5% level of significance.

LHHW elementary reaction mechanism (Methanol adsorption as rate limiting)

The increase in the number of kinetic rate constants although increases the degrees of freedom, but reduces statistical reliability due to lighter fitting with experimental data. Dossin et al.[2] developed a rate mechanism based on ER mechanism and adsorption of methanol as the rate determining step. The LHHW elementary mechanism with methanol adsorption as a rate limiting step involving three parameters, the rate coefficient for methanol adsorption k_{MeOH}, the adsorption equilibrium coefficient of the overall transesterification reaction K_{eq} and the adsorption equilibrium constant of the alcohols K_A, is thus statistically more reliable than the mechanism with the assumption of surface reaction as the rate limiting step. The kinetic rate constants obtained are shown in Table 8. Similar to all other mechanisms, adsorption of methanol is identified as the slowest and the rate determining step with the rate constants of 9.8×10^{-3}, 1.53×10^{-2}, 1.37×10^{-2} and 0.06, for $Mg_{0.81}Al$, $Mg_{1.38}Al$, $Mg_{1.82}Al$ and $Mg_{2.93}Al$ respectively. χ^2 of 0.052, 0.004, 0.033, and 0.011 achieved for $Mg_{0.81}Al$, $Mg_{1.38}Al$, $Mg_{1.82}Al$ and $Mg_{2.93}Al$ (Table 8) respectively is less than 1.34 required for 3 parameter models with 8 degrees of freedom for 99.5% level of significance[29]. Thus, LHHW mechanism with methanol adsorption as the rate determining step represents the given experimental observations in Appendix A, adequately.

Hattori elementary reaction mechanism (Methanol adsorption as rate limiting)

As discussed in the previous section the formation of intermediates is an important element in the Hattori elementary reaction model (Table 6) that differentiates it from the LHHW and ER mechanisms. The kinetic rate constants in the Hattori mechanism with methanol adsorption as the rate determining step are shown in the Table 8. The slowest reaction rate is the adsorption of

methanol (K_1) as expected, with the values of 4.45×10^{-3}, 5.09×10^{-3}, 8.11×10^{-3} and 0.014 for $Mg_{0.81}Al$, $Mg_{1.38}Al$, $Mg_{1.82}Al$ and $Mg_{2.93}Al$ respectively. The fastest reaction rates are K_3, corresponding to the reaction between adsorbed methanol and adsorbed triglyceride, 0.16 and 0.58 for $Mg_{0.81}Al$ and $Mg_{2.93}Al$ and K_4, the decomposition of intermediate species [$TsCH_3OH$*] (Table 3), 0.29 and 0.32 for $Mg_{1.38}Al$ and $Mg_{1.82}Al$, respectively. Table 8 indicates χ^2 of 0.05, 0.14, 0.30 and 0.009 for the four hydrotalcite catalysts with increasing Mg concentration, respectively. However, since the number of experimental points for this mechanism is the same as the number of kinetic parameters, statistical significance criteria cannot be applied to this model.

Comparison between kinetic models

In the previous section, the kinetic rate constants and the model fit χ^2 with the assumptions of quasi steady state, methanol adsorption and surface reaction as rate limiting steps in ER, LHHW and Hattori elementary reaction mechanisms, are determined in Table 8. The increase in the number of parameters increases the complexity of the model and reduces the limit on χ^2 for the statistical significance of the fit[29]. Hence, different models based on the statistical criterion P_{AB} as defined below[29] are further compared.

$$P_{AB} = \frac{\chi_A^2 / (N - n_A)}{\chi_B^2 / (N - n_B)} \qquad 11$$

Here, χ_A^2, χ_B^2 are the Chi-square, while n_A, n_B are the number of parameters, for model A and B respectively and N is the number of experimental points. If P_{AB} is lesser than one, model A fits the data better than model B and vice versa. The number of parameters for a model fit should be less than the number of experimental points by at least one. Overall reaction rate determined for Hattori elementary reaction with methanol adsorption as the rate determining step has 12 parameters which are the same as the number of experimental points. Hence, this model cannot be used for statistical analysis of this set of experimental data.

A comparison of performance using the statistical criterion P_{AB} between the kinetic models on the four hydrotalcite catalysts is shown in Table 9. The least number of parameters (in this case 3) are involved in LHHW and ER mechanisms with methanol adsorption as the rate determining

steps. Hence, these two mechanisms would be most recommended ones from statistical reliability point of view. At the same time, simpler, but adequately detailed reaction kinetics model can be integrated to multiscale reactor simulation frameworks[24]. By comparing the P_{AB} values in Table 9, the following sequences from the best performing to the worst performing mechanisms for individual catalysts are obtained, $Mg_{0.81}Al$: ER (Methanol adsorption) > LHHW (Surface reaction) > ER (Quasi steady state) > LHHW (Methanol adsorption); $Mg_{1.38}Al$: LHHW (Methanol adsorption) > ER (Methanol adsorption) > LHHW (Surface reaction) > ER (Quasi steady state); $Mg_{1.82}Al$: LHHW (Methanol adsorption) > ER (Quasi steady state) > LHHW (Surface reaction) > ER (Methanol adsorption); $Mg_{2.93}Al$: ER (Quasi steady state) > LHHW (Methanol adsorption) > ER (Methanol adsorption) > LHHW (Surface reaction); Hence, the LHHW (Methanol adsorption) provides consistently better representation of the experimental data compared to ER (methanol adsorption), except Mg0.81Al, to which ER (methanol adsorption) applies better than any other mechanism, illustrated in Table 9. Also, considering lower conversion resulting with lower molar fraction of Mg in hydrotalcite catalyst (Appendix A), biodiesel reactors are expected to incorporate hydrotalcite catalysts with higher molar fraction of Mg, in which cases LHHW with methanol adsorption as the rate determining step adequately and reliably represents the kinetic data. It also satisfies χ^2 limit of 1.34[29] for all four catalysts.

Table 9: Statistical comparison between kinetic models

4 Conclusions

Three kinetic mechanisms, ER, LHHW, and Hattori, based on assumptions of quasi steady state for the surface species and methanol adsorption and surface reaction as rate limiting steps were investigated for biodiesel production reaction between triglyceride and methanol over heterogeneous hydrotalcite catalyst[16]. These kinetic models were applied to represent four hydrotalcite catalysts with different molar compositions of Mg and Al. Activity coefficients were used to account for the non-ideal behaviour in this analysis. These kinetic models were observed to give a good fit with the experimental data. The models were compared based on the chi square χ^2 criteria and the number of parameters in the model. The LHHW kinetic mechanism

with methanol adsorption as the rate limiting step involved least number of parameters and was identified as the best fit for the experimental data.

To account for the effect of the surface coverage on catalysts, KMC simulations were performed. Further, mean field simulation of the bulk phase was combined with the surface KMC simulation in order to capture both the changes in the concentration profiles in the bulk as well as on the catalyst surface, simultaneously. The assumptions made for given mechanisms on all catalysts were reinforced by the results of surface coverage and bulk concentration evolutions with time. The most applicable reaction mechanism for individual catalysts was identified using the proposed strategy. Also, statistically most reliable mechanism was identified.

Acknowledgement:

Financial support from EPSRC (EP/D04829X/1) of the UK for undertaking this research is gratefully acknowledged.

Nomenclature

$[i]$	activity of specie *i*, mol m^{-3}
C_i	concentration of specie *i*, mol m^{-3}
$C_i(j)$	concentration of specie *i* at time point *j*, mol m^{-3}
$C_i^{experimental}(j)$	concentration of specie *i* obtained from experimental studies at time point *j*, mol m^{-3}
CH_3OH^*	Methanol adsorbed, dimensionless
CH_3OH	Methanol bulk, dimensionless
D^*	Diglyceride adsorbed, dimensionless
D	Diglyceride bulk, dimensionless
G^*	Glycerol adsorbed, dimensionless
G	Glycerol bulk, dimensionless
K_A	adsorption equilibrium constant of the alcohols present, m^3 mol^{-1}
K_{eq}	equilibrium coefficient of the overall transesterification reaction, dimensionless
k_{MeOH}	rate coefficient for methanol adsorption, s^{-1}

k_j	forward reaction rate constant for elementary reaction *j*, variable units
K_j	Equilibrium constant for elementary reaction *j*, dimensionless
l_i	UNIFAC method parameter for specie *i*
M^*	Monoglyceride adsorbed, dimensionless
M	Monoglyceride bulk, dimensionless
$MeOl$	Methyl Oleate bulk, dimensionless
$nspc$	number of species, dimensionless
$ntime$	total number of experimental values, dimensionless
P_{AB}	statistical criteria to compare model *A* and *B*, dimensionless
n_A	number of parameters in model *A*, dimensionless
n_B	number of parameters in model *B*, dimensionless
N	number of experimental points, dimensionless
Q_p	group area parameter
q_i	molecular van der Waals surface area
r_j	reaction rate for j^{th} reaction, mol m^{-3}
r	overall reaction rate expression, mol m^{-3}
R_p	group volume
$RSSQ$	residual sum of squares, dimensionless
R_i	reaction rate of the specie *i*
R_T	rate of consumption of *T*, mol m^{-3}
R_D	rate of consumption of *D*, mol m^{-3}
R_M	rate of consumption of *M*, mol m^{-3}
R_{CH_3OH}	Rate of consumption of CH_3OH, mol m^{-3}
R_G	rate of consumption of *G*, mol m^{-3}
R_{MeOl}	rate of generation of *MeOl*, mol m^{-3}
s_i	molecular van der Waals volume
S_p	group area parameter
T	Triglyceride bulk, dimensionless
Te	Temperature, K
t	Time, s

$v_p^{(i)}$	number of *p* groups present in molecule *i*, dimensionless
x_i	mole fraction of specie *i*, dimensionless
*	empty surface site, dimensionless

Symbols

γ_i^C	combinatorial factor for activity coefficient calculation, dimensionless
γ_i^R	residual factor for activity coefficient calculation, dimensionless
γ_i	activity coefficient of species *i*, dimensionless
χ^2	chi square, dimensionless
Ψ_{ip} , $a_{ii'}$	group interaction parameters
Φ_i	segment fraction for specie *i*, dimensionless
θ_i	area fraction for specie *i*, dimensionless
Γ_p	group residual activity coefficient, dimensionless
$\Gamma_p^{(i)}$	residual coefficient of group *p* in reference solution containing only molecules of type *i*, dimensionless

References

1. Narasimharao, K.; Lee, A.; Wilson, K., Catalysts in production of biodiesel: A review. *Journal of Biobased Materials and Bioenergy* **2007,** 1, (1), 19-30.
2. Dossin, T. F.; Reyniers, M. F.; Berger, R. J.; Marin, G. B., Simulation of heterogeneously MgO-catalyzed transesterification for fine-chemical and biodiesel industrial production. *Applied Catalysis B-Environmental* **2006,** 67, (1-2), 136-148.
3. Crocker, M. In *Development of Heterogeneous Catalysts for Bio-diesel Production*, Tri-State Catalysis Society Symposium, Lexington, KY, 2006; Lexington, KY, 2006.
4. Ngaosuwan, K.; Lotero, E.; Suwannakarn, K.; Goodwin, J. G. J.; Praserthdam, P., Hydrolysis of Triglycerides using Solid Acid Catalysts. *Industrial & Engineering Chemistry Research* **2009,** 48, 4757-4767.
5. Vyas, A. P.; Subrahmanyam, N.; Patel, P. A., Production of biodiesel through transesterification of Jatropha oil using KNO3/Al2O3 solid catalyst. *Fuel* **2009,** 88, (4), 625-628.
6. Benjapornkulaphong, S.; Ngamcharussrivichai, C.; Bunyakiat, K., Al2O3-supported alkali and alkali earth metal oxides for transesterification of palm kernel oil and coconut oil. *Chemical Engineering Journal* **2009,** 145, (3), 468-474.

7. de Caland, L. B.; Santos, L. S. S.; de Moura, C. V. R.; de Moura, E. M., Preparation and Study of Bimetallic Compounds Efficiency in the Synthesis of Biodiesel Fuel. *Catalysis Letters* **2009,** 128, (3-4), 392-400.
8. Singh, A. K.; Fernando, S. D., Transesterification of soybean oil using heterogeneous catalysts. *Energy & Fuels* **2008,** 22, (3), 2067-2069.
9. Verziu, M.; Cojocaru, B.; Hu, J. C.; Richards, R.; Ciuculescu, C.; Filip, P.; Parvulescu, V. I., Sunflower and rapeseed oil transesterification to biodiesel over different nanocrystalline MgO catalysts. *Green Chemistry* **2008,** 10, (4), 373-381.
10. Brito, A.; Borges, M. E.; Otero, N., Zeolite Y as a heterogeneous catalyst in biodiesel fuel production from used vegetable oil. *Energy & Fuels* **2007,** 21, (6), 3280-3283.
11. Dalai, A. K.; Kulkarni, M. G.; Meher, L. C., Biodiesel productions from vegetable oils using heterogeneous catalysts and their applications as lubricity additives. *2006 IEEE EIC Climate Change Conference, Vols 1 and 2* **2006**, 517-524.
12. Di Serio, M.; Cozzolino, M.; Giordano, M.; Tesser, R.; Patrono, P.; Santacesaria, E., From homogeneous to heterogeneous catalysts in biodiesel production. *Industrial & Engineering Chemistry Research* **2007,** 46, (20), 6379-6384.
13. Di Serio, M.; Ledda, M.; Cozzolino, M.; Minutillo, G.; Tesser, R.; Santacesaria, E., Transesterification of soybean oil to biodiesel by using heterogeneous basic catalysts. *Industrial & Engineering Chemistry Research* **2006,** 45, (9), 3009-3014.
14. Cantrell, D. G.; Gillie, L. J.; Lee, A. F.; Wilson, K., Structure-reactivity correlations in MgAl hydrotalcite catalysts for biodiesel synthesis. *Applied Catalysis A-General* **2005,** 287, (2), 183-190.
15. Macedo, C. C. S.; Abreu, F. R.; Tavares, A. P.; Alves, M. B.; Zara, L. F.; Rubim, J. C.; Suarez, P. A. Z., New heterogeneous metal-oxides based catalyst for vegetable oil trans-esterification. *Journal of the Brazilian Chemical Society* **2006,** 17, (7), 1291-1296.
16. Dossin, T. F.; Reyniers, M. F.; Marin, G. B., Kinetics of heterogeneously MgO-catalyzed transesterification. *Applied Catalysis B-Environmental* **2006,** 62, (1-2), 35-45.
17. Raimondeau, S.; Vlachos, D. G., Recent developments on multiscale, hierarchical modeling of chemical reactors. *Chemical Engineering Journal* **2002,** 90, 3.
18. Karpov, E. G.; Chaichenets, S.; Liu, W. K.; Qian, D., Mechano-kinetic coupling approach for materials with dynamic internal structure. *Philosophical Magazine Letters* 90, (7), 471-480.
19. Levchenko, I.; Ostrikov, K.; Khachan, J.; Vladimirov, S. V., Growth of carbon nanocone arrays on a metal catalyst: The effect of carbon flux ionization. *Physics of Plasmas* **2008,** 15, (10).
20. Majumder, D.; Broadbelt, L. J., A multiscale scheme for modeling catalytic flow reactors. *AIChE Journal* **2006,** 52, (12), 4214-4228.
21. Vlachos, D. G.; Mhadeshwar, A. B.; Kaisare, N. S., Hierarchical multiscale model-based design of experiments, catalysts, and reactors for fuel processing. *Computers & Chemical Engineering* **2006,** 30, (10-12), 1712-1724.
22. Raimondeau, S.; Vlachos, D. G., The role of adsorbate-layer nonuniformities in catalytic reactor design: multiscale simulations for CO oxidation on Pt. *Computers & Chemical Engineering* **2002,** 26, (7-8), 965-980.
23. Reese, J. S.; Raimondeau, S.; Vlachos, D. G., Monte Carlo Algorithms for Complex Surface Reaction Mechanisms: Efficiency and Accuracy. *Journal of Computational Physics* **2001,** 173, (1), 302-321.

24. Kapil, A.; Bhat, S. A.; Sadhukhan, J., Multiscale characterization framework for sorption enhanced reaction processes. *Aiche Journal* **2008,** 54, (4), 1025-1036.
25. Bhat, S. A.; Sharma, R.; Gupta, S. K., Simulation and optimization of the continuous tower process for styrene polymerization. *Journal of Applied Polymer Science* **2004,** 94, (2), 775-788.
26. Xu, M.; Bhat, S.; Smith, R.; Stephens, G.; Sadhukhan, J., Multi-objective optimisation of metabolic productivity and thermodynamic performance. *Computers and Chemical Engineering* **2009,** 33, (9), 1438-1450.
27. Reid, R. C.; Praustnitz, J. M.; Poling, B. E., *The Properties of Gases and Liquids*. 4th ed.; MacGraw-Hill, New York: 1987.
28. Haupt, R.; Haupt, S. E., *Practical Genetic Algorithms* 2ed.; John Wiley & Sons Inc New York, 2004; p 253.
29. Kreyszig, E., *ADVANCED ENGINEERING MATHEMATICS*. 8 ed.; John Wiley & Sons, Inc.: New York, 1999.

Appendix A

Experimental data

Wilson and coworkers[14] developed a series of hydrotalcite catalyst with the general formulae of $\left[Mg_{(1-x)}Al_x(OH)_2\right]^{x+}(CO_3)_{x/n}{}^{2-}$ with x in a range of 0.25–0.55. Table 10 shows the nominal Mg:Al ratio along with the distribution of Mg and Al in the bulk and surface of these catalysts. The effect of increasing Mg fraction on the activity and surface area of these hydrotalcite catalysts is shown in Table 10. With the increase in Mg content the surface area of the catalyst initially decreases and then increases. The increase in activity with the increase in the Mg molar fraction led to higher conversion of triglyceride and more production of methyl oleate.

The transesterification reactions were performed in stirred batch reactor at 333 K using 0.01 mol (3 cm^3) of glyceryl tributyrate and 0.3036 mol (12.5 cm^3) methanol. The batch reactor was run for 3 hours.

Table 10: Properties of hyrotalcite catalysts[14]

Appendix B

Genetic Algorithm (GA)

The GA algorithm used in this simulation is based on the studies by Bhat et al.[25], Xu et al.[26] and Haupt and Haupt[28]. The algorithm is implemented in MATLAB.

- Specify the initial inputs to the genetic algorithm. Population size is 1000, while maximum number of iterations is 100000. The bounds of control variables (rate constants) are specified between 10^{-1} and 2 orders of magnitude.
- Initial chromosomes are generated, with each chromosome representing a feasible solution in terms of decision variables.
- The objective function is generated for these sets of rate constants.
- The chromosomes are ranked based on the objective function.
- The best x percent (50%) chromosomes are kept for the next iteration.
- Generate a new set of chromosomes by mutation, crossover in remaining chromosomes. The cost of the new chromosomes is evaluated on the objective function.
- Simulations are repeated until objective function is a very low value within the expected tolerance limits or the maximum number of iterations (100000) is exceeded.

Appendix C

Prediction of activity coefficients of species

In the UNIFAC method the activity coefficient (γ_i) is made up of two parts: the first part provides the contribution due to molecular shape, combinatorial factor (γ_i^C), and the other due to the interaction between molecules, residual factor (γ_i^R), respectively [16].

$$\ln \gamma_i = \ln \gamma_i^C + \ln \gamma_i^R \qquad 12$$

$$\ln \gamma_i^C = \ln \frac{\Phi_i}{x_i} + 5q_i \ln \frac{\theta_i}{\Phi_i} + l_i - \frac{\Phi_i}{x_i} \sum_{i'}^{nspc} x_{i'} l_{i'} \qquad 13$$

Here, x_i is the mole fraction, Φ_i and θ_i are the segment and area fractions for specie *i* respectively.

$$\ln \gamma_i^R = \sum_{p}^{all\ groups} v_p^{(i)} \left(\ln \Gamma_p - \ln \Gamma_p^{(i)} \right) \qquad 14$$

In these equations, Γ_p , $\Gamma_p^{(i)}$ are the group residual activity coefficient and the residual coefficient of group *p* in reference solution containing only molecules of type *i*.

$$\theta_i = \frac{x_i q_i}{\sum_{i'} x_{i'} q_{i'}} \quad \Phi_i = \frac{x_i s_i}{\sum_{i'} x_{i'} s_{i'}} \qquad 15$$

s_i and q_i are the measure of molecular van der Waals volume and molecular surface area respectively.

$$l_i = 5(s_i - q_i) - (s_i - 1)$$

$$s_i = \sum_p v_p^{(i)} S_p \quad q_i = \sum_p v_p^{(i)} Q_p \qquad 16$$

S_p and Q_p are group volume and area parameters, $v_p^{(i)}$ is the number of *p* groups present in molecule *i*. The group activity coefficient Γ_p is a function of area parameter Q_p , area fraction θ_i and the group interaction parameter Ψ_{ip} and $a_{ii'}$. *Te* is the temperature.

$$\ln \Gamma_p = Q_p \left\{ 1 - \ln \left(\sum_i^{nspc.} \theta_i \Psi_{ip} \right) - \sum_i^{nspc} \frac{\theta_i \Psi_{pi}}{\sum_{i'}^{nspc} \theta_i \Psi_{i'i}} \right\}$$

$$\Psi_{ii'} = \exp\left(-\frac{a_{ii'}}{Te}\right) \quad \textbf{17}$$

List of figures

List of tables

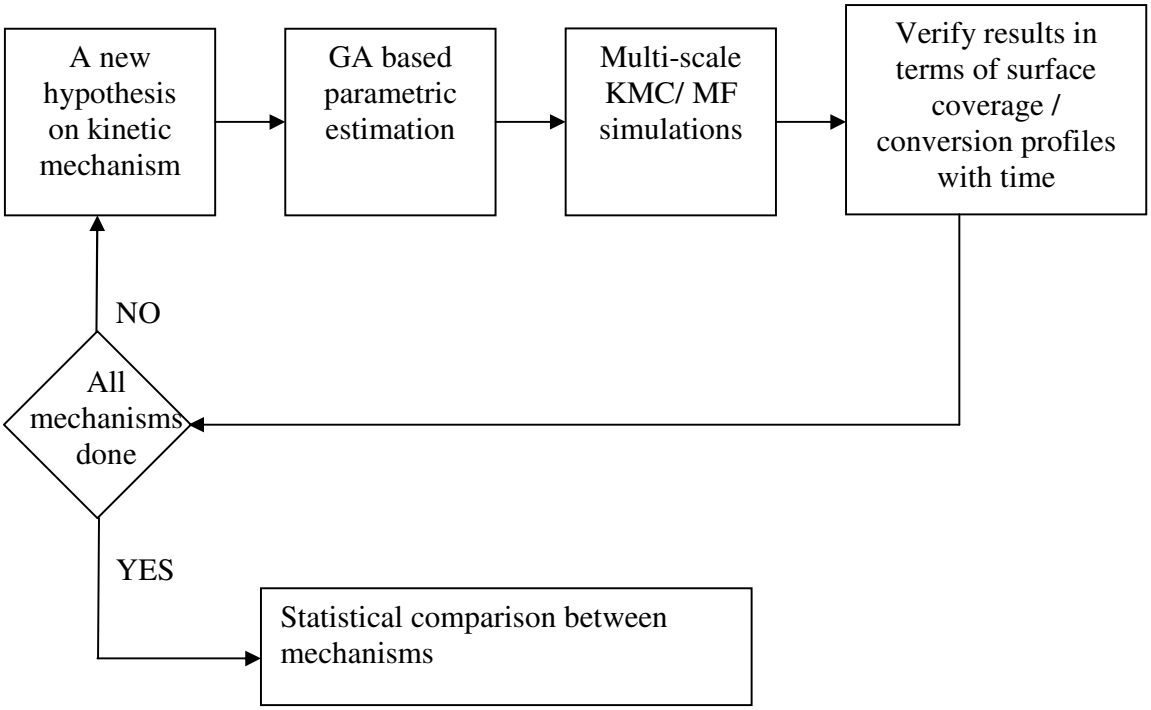

Figure 6: Overall methodology to determine reaction mechanisms

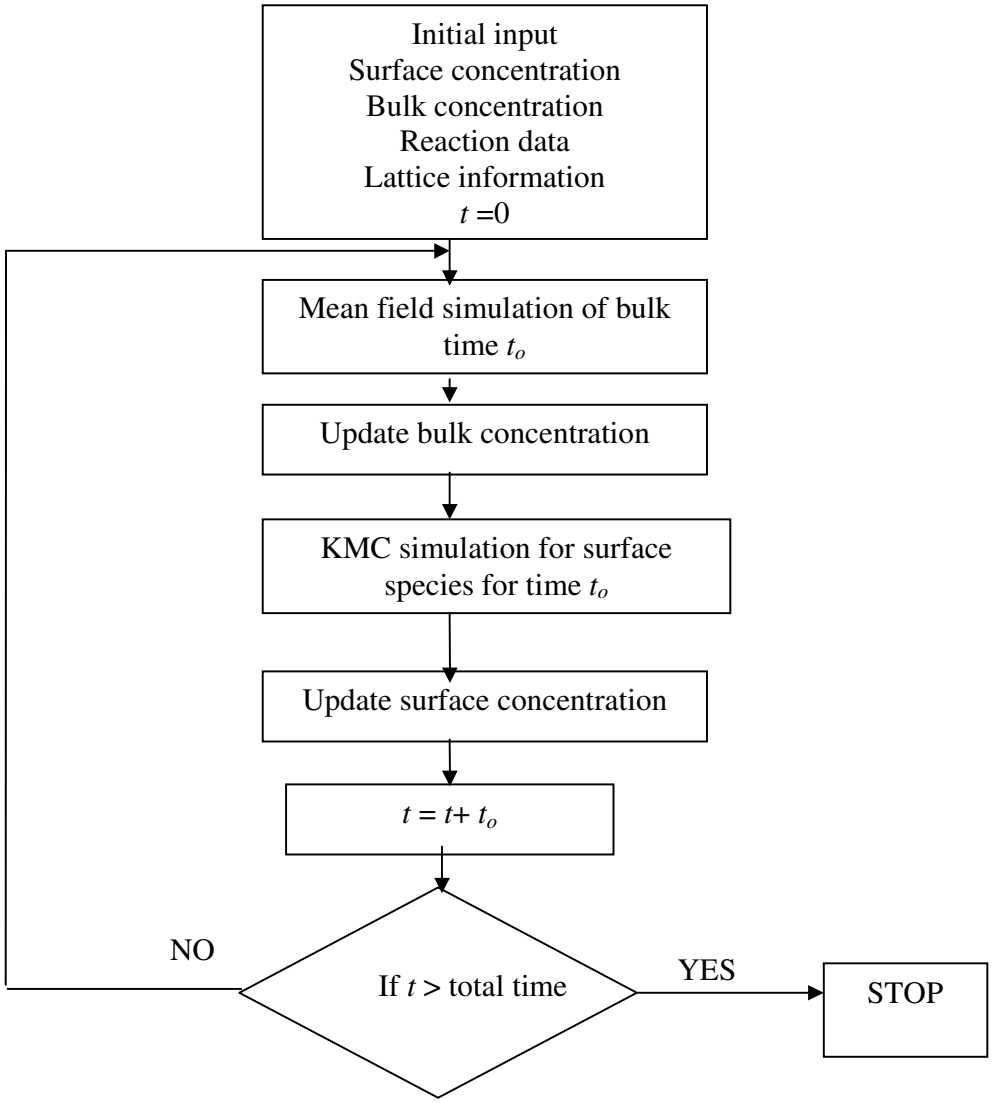

Figure 7: Multi-scale KMC/MF simulation methodology

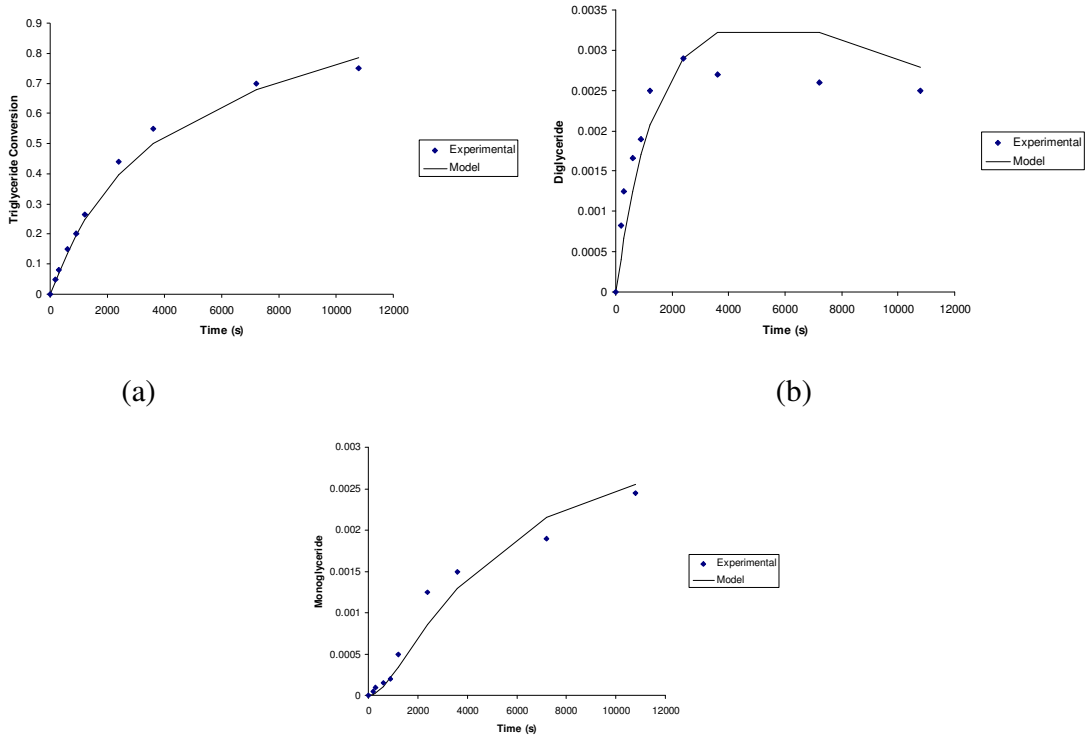

Figure 8: Comparison between (a) conversion of Triglyceride (T); (b) moles of Diglyceride (D); and (c) moles of Monoglyceride (M); for $Mg_{2.93}Al$ hydrotalcites obtained from ER quasi steady state model

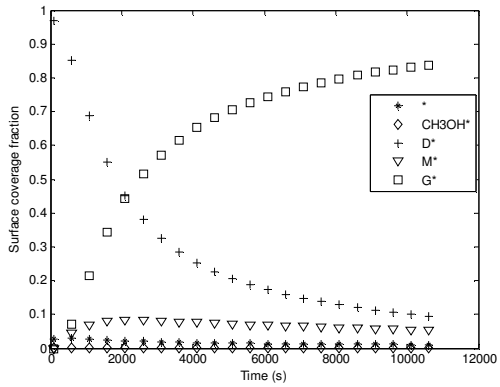

Figure 9: Time evolution of surface species from KMC simulation

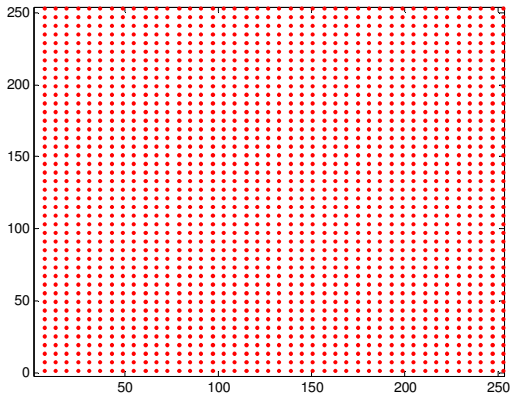

(a)

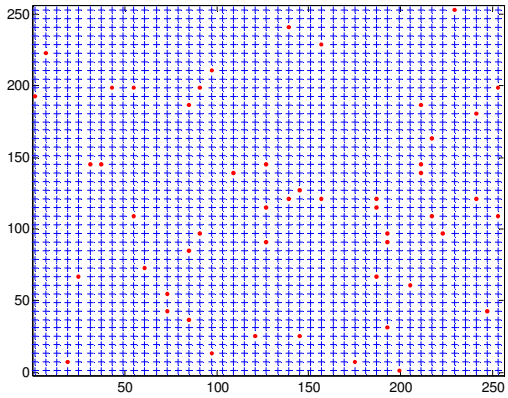

(b)

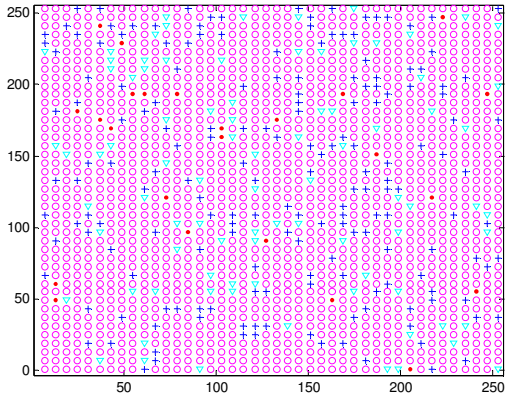

(c)

Figure 10: Evolution of catalyst surface from KMC simulations; *(.), CH3OH*(~), D*(+), M*(ω), G*(°). Case (a) * (100%), CH3OH*(0), D*(0), M*(0), G*(0) at t=0s; Case (b) * (2.9%), CH3OH*(0.07%), D*(97.1%), M*(0), G*(0) at t=2000s ; Case (c) * (5.4%), CH3OH*(0.1%), D*(43.9%), M*(25.3%), G*(25.3%) at t=10800s;

Table 11: Activity coefficients of species

i	T	D	M	G	CH_3OH	$MeOl$
γ_i	3.15	0.85	0.49	0.89	1.01	2.98

Table 12: Elementary reactions in ER mechanism

$*+CH_3OH \Leftrightarrow CH_3OH*$	**(a)**	
$CH_3OH*+T \Leftrightarrow D*+MeOl$	**(b)**	
$CH_3OH*+D \Leftrightarrow M*+MeOl$	**(c)**	
$CH_3OH*+M \Leftrightarrow G*+MeOl$	**(d)**	
$D* \Leftrightarrow D+*$	**(e)**	
$M* \Leftrightarrow M+*$	**(f)**	
$G* \Leftrightarrow G+*$	**(g)**	**18**

Table 13: Kinetic reaction rate expressions for ER quasi steady state mechanism

Rate of consumption of T	$R_T = \left(\frac{k_2[T]}{1+\left(\frac{k_2[T]+k_3[D]+k_4[M]}{k_1[CH_3OH]} \right)+\frac{k_2[D]}{k_6}+\frac{k_2[T]}{k_5}+\frac{k_4[M]}{k_7}} \right)$
Rate of consumption of D	$R_D = \left(\frac{k_3[D]-k_2[T]}{1+\left(\frac{k_2[T]+k_3[D]+k_4[M]}{k_1[CH_3OH]} \right)+\frac{k_2[D]}{k_6}+\frac{k_2[T]}{k_5}+\frac{k_4[M]}{k_7}} \right)$
Rate of consumption of M	$R_M = \left(\frac{k_4[M]-k_3[D]}{1+\left(\frac{k_2[T]+k_3[D]+k_4[M]}{k_1[CH_3OH]} \right)+\frac{k_2[D]}{k_6}+\frac{k_2[T]}{k_5}+\frac{k_4[M]}{k_7}} \right)$
Rate of consumption of CH_3OH	$R_{CH_3OH} = \left(\frac{-(k_5[D]+k_3[T]+k_7[M])}{1+\left(\frac{k_2[T]+k_3[D]+k_4[M]}{k_1[CH_3OH]} \right)+\frac{k_2[D]}{k_6}+\frac{k_2[T]}{k_5}+\frac{k_4[M]}{k_7}} \right)$
Rate of change for G	$R_G = \left(\frac{k_7 k_1[CH_3OH]}{k_3[T]+k_5[D]+k_7[M]} \right)$
Rate of generation of $MeOl$	$R_{MeOl} = \left(\frac{(k_5[D]+k_3[T]+k_7[M])}{1+\left(\frac{k_2[T]+k_3[D]+k_4[M]}{k_1[CH_3OH]} \right)+\frac{k_2[D]}{k_6}+\frac{k_2[T]}{k_5}+\frac{k_4[M]}{k_7}} \right)$

Table 14: Elementary reactions in LHHW mechanism

Elementary reactions	*Equilibrium reaction constants*
$*+CH_3OH \Leftrightarrow CH_3OH*$	$K_1 = \frac{[CH_3OH*]}{[*][CH_3OH]}$
$T+* \Leftrightarrow T*$	$K_2 = \frac{[T*]}{[*][T]}$
$CH_3OH*+T* \Leftrightarrow D*+MeOl*$	$K_3 = \frac{[D*][MeOl*]}{[CH_3OH*][T*]}$
$CH_3OH*+D* \Leftrightarrow M*+MeOl*$	$K_4 = \frac{[M*][MeOl*]}{[CH_3OH*][D*]}$
$CH_3OH*+M* \Leftrightarrow G*+MeOl*$	$K_5 = \frac{[G*][MeOl*]}{[CH_3OH*][M*]}$
$MeOl+* \Leftrightarrow MeOl*$	$K_6 = \frac{[MeOl*]}{[*][MeOl]}$
$D+* \Leftrightarrow D*$	$K_7 = \frac{[D*]}{[*][D]}$
$M+* \Leftrightarrow M*$	$K_8 = \frac{[M*]}{[*][M]}$
$G+* \Leftrightarrow G*$	$K_9 = \frac{[G*]}{[*][G]}$

Table 15: Elementary reaction rate expressions for LHHW mechanism with surface reaction as rate limiting

Rate determining reaction	*Overall reaction rate*
$*+CH_3OH \Leftrightarrow CH_3OH*$	$r_1 = \frac{k_1\left([CH_3OH] - \frac{1}{K_1}\frac{K_6K_7}{K_3K_2}\frac{[D][MeOl]}{[T]}\right)}{\left(1+\frac{K_6K_7}{K_3K_2}\frac{[D][MeOl]}{[T]}+K_6[MeOl]+K_2[T]+K_7[D]+K_8[M]+K_9[G]\right)}$
$T+*\Leftrightarrow T*$	$r_2 = \frac{k_2\left([T] - \frac{1}{K_2}\frac{K_6K_7}{K_3K_1}\frac{[D][MeOl]}{[CH_3OH]}\right)}{\left(1+K_1[CH_3OH]+K_6[MeOl]+\frac{K_6K_7}{K_3K_1}\frac{[D][MeOl]}{[CH_3OH]}+K_7[D]+K_8[M]+K_9[G]\right)}$
$CH_3OH*+T* \Leftrightarrow D*+MeOl*$	$r_3 = \frac{k_3\left(K_1K_2[CH_3OH][T] - \frac{1}{K_3}K_7K_6[D][MeOl]\right)}{(1+K_1[CH_3OH]+K_6[MeOl]+K_2[T]+K_7[D]+K_8[M]+K_9[G])^2}$
$CH_3OH*+D* \Leftrightarrow M*+MeOl*$	$r_4 = \frac{k_4\left(K_1K_7[CH_3OH][D] - \frac{1}{K_4}K_8K_6[M][MeOl]\right)}{(1+K_1[CH_3OH]+K_6[MeOl]+K_2[T]+K_7[D]+K_8[M]+K_9[G])^2}$
$CH_3OH*+M* \Leftrightarrow G*+MeOl*$	$r_5 = \frac{k_5\left(K_1K_8[CH_3OH][M] - \frac{1}{K_5}K_9K_6[G][MeOl]\right)}{(1+K_1[CH_3OH]+K_6[MeOl]+K_2[T]+K_7[D]+K_8[M]+K_9[G])^2}$
$MeOl* \Leftrightarrow MeOl+*$	$r_6 = \frac{k_6\left(\frac{K_3K_2K_1[T][CH_3OH]}{K_7[D]} - K_6[MeOl]\right)}{\left(1+K_1[CH_3OH]+\frac{K_3K_2K_1[T][CH_3OH]}{K_7[D]}+K_2[T]+K_7[D]+K_8[M]+K_9[G]\right)}$
$D* \Leftrightarrow D+*$	$r_7 = \frac{k_7\left(\frac{K_3K_2K_1[T][CH_3OH]}{K_6[MeOl]} - K_7[D]\right)}{\left(1+K_1[CH_3OH]+K_6[MeOl]+K_2[T]+\frac{K_3K_2K_1[T][CH_3OH]}{K_6[MeOl]}+K_8[M]+K_9[G]\right)}$

$M^{*} \Leftrightarrow M + *$	$r_8 = \frac{k_8\left(\frac{K_4 K_1 K_7 [D][CH_3OH]}{K_6[MeOl]} - K_8[M]\right)}{\left(1 + K_1[CH_3OH] + K_6[MeOl] + K_2[T] + K_7[D] + \frac{K_4 K_1 K_7 [D][CH_3OH]}{K_6[MeOl]} + K_9[G]\right)}$
$G^{*} \Leftrightarrow G + *$	$r_9 = \frac{k_9\left(\frac{K_5 K_8 K_1 [M][CH_3OH]}{K_6[MeOl]} - K_9[G]\right)}{\left(1 + K_1[CH_3OH] + K_6[MeOl] + K_2[T] + K_7[D] + K_8[M] + \frac{K_5 K_8 K_1 [M][CH_3OH]}{K_6[MeOl]}\right)}$

Table 16: Elementary reactions in Hattori mechanism

Elementary reactions	*Equilibrium reaction constants*
$*+CH_3OH \Leftrightarrow CH_3OH*$	$K_1 = \frac{[CH_3OH*]}{[*][CH_3OH]}$
$T+* \Leftrightarrow T*$	$K_2 = \frac{[T*]}{[*][T]}$
$CH_3OH*+T* \Leftrightarrow [TsCH_3OH]*+*$	$K_3 = \frac{[*][TsCH_3OH*]}{[CH_3OH*][T*]}$
$[TsCH_3OH]* \Leftrightarrow D*+ MeOl$	$K_4 = \frac{[D*][MeOl]}{[TsCH_3OH*]}$
$CH_3OH*+D* \Leftrightarrow [DsCH_3OH]*+*$	$K_5 = \frac{[*][DsCH_3OH*]}{[CH_3OH*][D*]}$
$[DsCH_3OH]* \Leftrightarrow M*+ MeOl$	$K_6 = \frac{[M*][MeOl]}{[DsCH_3OH*]}$
$CH_3OH*+M* \Leftrightarrow [MsCH_3OH]*+*$	$K_7 = \frac{[*][MsCH_3OH*]}{[CH_3OH*][M*]}$
$[MsCH_3OH]* \Leftrightarrow G*+ MeOl$	$K_8 = \frac{[G*][MeOl]}{[MsCH_3OH*]}$
$D+* \Leftrightarrow D*$	$K_9 = \frac{[D*]}{[*][D]}$
$M+* \Leftrightarrow M*$	$K_{10} = \frac{[M*]}{[*][M]}$
$G+* \Leftrightarrow G*$	$K_{11} = \frac{[G*]}{[*][G]}$

Table 17: Elementary reaction rate expressions for Hattori mechanism with methanol adsorption as rate limiting

Rate determining reaction	*Overall reaction rate*
+CH3OH⇔ CH3OH	$r_1 = \frac{k_1\left([CH_3OH] - \frac{1}{K_1}\frac{K_9}{K_4K_3K_2}\frac{[D][MeOl]}{[T]}\right)}{\left(1+\frac{K_9}{K_4K_3K_2}\frac{[D][MeOl]}{[T]}+\frac{K_9[D][MeOl]}{K_4}+\frac{K_{10}[M][MeOl]}{K_6}+\frac{K_{11}[G][MeOl]}{K_8}+K_2[T]+K_9[D]+K_{10}[M]+K_{11}[G]\right)}$
T+ ⇔ T**	$r_2 = \frac{k_2\left([T] - \frac{1}{K_2}\frac{K_9}{K_4K_3K_1}\frac{[D][MeOl]}{[CH_3OH]}\right)}{\left(1+K_1[CH_3OH]+\frac{K_9[D][MeOl]}{K_4}+\frac{K_{10}[M][MeOl]}{K_6}+\frac{K_{11}[G][MeOl]}{K_8}+\frac{K_9}{K_4K_3K_1}\frac{[D][MeOl]}{[CH_3OH]}+K_9[D]+K_{10}[M]+K_{11}[G]\right)}$
CH_3OH+T* ⇔ [$TsCH_3OH$]* +**	$r_3 = \frac{k_3\left(K_1K_2[CH_3OH][T] - \frac{1}{K_3}\frac{K_9}{K_4}[D][MeOl]\right)}{\left(1+K_1[CH_3OH]+\frac{K_9[D][MeOl]}{K_4}+\frac{K_{10}[M][MeOl]}{K_6}+\frac{K_{11}[G][MeOl]}{K_8}+K_2[T]+K_9[D]+K_{10}[M]+K_{11}[G]\right)^2}$
[$TsCH_3OH$] ⇔ D*+ MeOl*	$r_4 = \frac{k_4\left(K_3K_2K_1[CH_3OH][T] - \frac{1}{K_4}K_9[D][MeOl]\right)}{\left(1+K_1[CH_3OH]+K_3K_2K_1[CH_3OH][T]+\frac{K_{10}[M][MeOl]}{K_6}+\frac{K_{11}[G][MeOl]}{K_8}+K_2[T]+K_9[D]+K_{10}[M]+K_{11}[G]\right)}$
CH_3OH+D* ⇔ [$DsCH_3OH$] *+**	$r_5 = \frac{k_5\left(K_1K_9[CH_3OH][D] - \frac{1}{K_5}\frac{K_{10}}{K_6}[M][MeOl]\right)}{\left(1+K_1[CH_3OH]+\frac{K_9[D][MeOl]}{K_4}+\frac{K_{10}[M][MeOl]}{K_6}+\frac{K_{11}[G][MeOl]}{K_8}+K_2[T]+K_9[D]+K_{10}[M]+K_{11}[G]\right)^2}$
*[$DsCH_3OH$] * ⇔ M*+ MeOl*	$r_6 = \frac{k_6\left(K_5K_9K_1[CH_3OH][D] - \frac{1}{K_6}K_{10}[M][MeOl]\right)}{\left(1+K_1[CH_3OH]+\frac{K_9[D][MeOl]}{K_4}+K_5K_9K_1[CH_3OH][D]+\frac{K_{11}[G][MeOl]}{K_8}+K_2[T]+K_9[D]+K_{10}[M]+K_{11}[G]\right)}$
CH_3OH+M* ⇔ [$MsCH_3OH$] *+**	$r_7 = \frac{k_7\left(K_1K_{10}[CH_3OH][M] - \frac{1}{K_7}\frac{K_{11}}{K_8}[G][MeOl]\right)}{\left(1+K_1[CH_3OH]+\frac{K_9[D][MeOl]}{K_4}+\frac{K_{10}[M][MeOl]}{K_6}+\frac{K_{11}[G][MeOl]}{K_8}+K_2[T]+K_9[D]+K_{10}[M]+K_{11}[G]\right)^2}$
*[$MsCH_3OH$] * ⇔ G*+*	$r_8 = \frac{k_8\left(K_7K_{10}K_1[CH_3OH][M] - \frac{1}{K_8}K_{11}[G][MeOl]\right)}{\left(1+K_1[CH_3OH]+\frac{K_9[D][MeOl]}{K_4}+\frac{K_{10}[M][MeOl]}{K_6}+K_7K_{10}K_1[CH_3OH][M]+K_2[T]+K_9[D]+K_{10}[M]+K_{11}[G]\right)}$

MeOl	
D ⇔ D+**	$$r_9 = \frac{k_9\left(\frac{K_{10}[M][MeOl]}{K_5K_6K_1[CH_3OH]} - K_9[D]\right)}{\left(1 + K_1[CH_3OH] + \frac{K_9[D][MeOl]}{K_4} + \frac{K_{10}[M][MeOl]}{K_6} + \frac{K_{11}[G][MeOl]}{K_8} + K_2[T] + \frac{K_{10}[M][MeOl]}{K_5K_6K_1[CH_3OH]} + K_{10}[M] + K_{11}[G]\right)}$$
M⇔ M+**	$$r_{10} = \frac{k_{10}\left(\frac{K_{11}[G][MeOl]}{K_7K_8K_1[CH_3OH]} - K_{10}[M]\right)}{\left(1 + K_1[CH_3OH] + \frac{K_9[D][MeOl]}{K_4} + \frac{K_{10}[M][MeOl]}{K_6} + \frac{K_{11}[G][MeOl]}{K_8} + K_2[T] + K_9[D] + \frac{K_{11}[G][MeOl]}{K_7K_8K_1[CH_3OH]} + K_{11}[G]\right)}$$
G⇔ G+**	$$r_{11} = \frac{k_{11}\left(K_8K_7K_1K_{10}\frac{[CH_3OH][M]}{[MeOl]} - K_{11}[G]\right)}{\left(1 + K_1[CH_3OH] + \frac{K_9[D][MeOl]}{K_4} + \frac{K_{10}[M][MeOl]}{K_6} + \frac{K_{11}[G][MeOl]}{K_8} + K_2[T] + K_9[D] + K_{10}[M] + K_8K_7K_1K_{10}\frac{[CH_3OH][M]}{[MeOl]}\right)}$$

Table 18: Prediction of kinetic rate constants and χ^2 for different mechanisms and catalysts

ER quasi steady state

k	$Mg_{0.81}Al$	$Mg_{1.38}Al$	$Mg_{1.82}Al$	$Mg_{2.93}Al$
1	1.01E-05	4.43E-06	0.0001	0.0001
2	0.0101	0.0495	0.0980	0.0390
3	0.1674	0.0271	0.1186	0.1741
4	0.3307	0.4590	0.0274	0.3587
5	0.0381	0.0519	0.0504	0.0564
6	0.0086	0.1305	0.1260	0.1579
7	0.088	0.0031	0	0.0082
χ^2	0.0174	0.2661	0.0218	0.0044

ER methanol adsorption as rate determining

K	$Mg_{0.81}Al$	$Mg_{1.38}Al$	$Mg_{1.82}Al$	$Mg_{2.93}Al$
k_f	1.60E-06	1.71E-06	7.33E-06	7.12E-06
K_A	0.0184	0.0130	0.0437	0.0206
χ^2	0.0276	0.0322	0.1772	0.0129

LHHW surface reaction as rate limiting

K	$Mg_{0.81}Al$	$Mg_{1.38}Al$	$Mg_{1.82}Al$	$Mg_{2.93}Al$
1	5.97E-05	1.00E-04	3.30E-05	0.0001
2	0.0850	0.0533	0.1353	0.1665
3	0.1613	0.1873	0.1509	0.1784
4	0.3729	0.4816	0.0319	0.4442
5	0.0764	0.0456	0.0307	0.0326
6	0.1709	0.0128	0.0121	0.0608
7	0.0006	0.0026	0.0041	0.0013
8	0.0319	0.0402	0.0118	0.0499
9	0.0927	0.0621	0.0399	0.0522
k_1	0.0195	0.0226	0.0664	0.0202
χ^2	0.0061	0.0203	0.0092	0.0129

LHHW methanol adsorption as rate limiting

K	$Mg_{0.81}Al$	$Mg_{1.38}Al$	$Mg_{1.82}Al$	$Mg_{2.93}Al$
k_f	9.80E-03	1.53E-02	1.37E-02	0.0611
K_A	0.0003	0.0125	0.0223	0.0009
K_{eq}	0.0312	0.0009	0.0013	0.0348
χ^2	0.0521	0.0041	0.0333	0.0114

Hattori methanol adsorption as rate determining

K	$Mg_{0.81}Al$	$Mg_{1.38}Al$	$Mg_{1.82}Al$	$Mg_{2.93}Al$
1	4.45E-03	5.09E-03	8.11E-03	0.0140
2	0.0945	0.1376	0.0216	1.4572
3	0.1642	0.1607	0.1662	0.5854
4	0.1218	0.2941	0.3244	0.4282

5	0.0119	0.0498	0.0146	0.0708
6	0.1344	0.1392	0.1893	0.0289
7	0.0186	0.0073	0.0684	0.0639
8	0.0750	0.0318	0.0194	0.0648
9	0.0001	0.0018	8.34E-05	0.0151
10	0.0502	0.0024	0.0887	0.0782
11	0.0644	0.0637	0.0130	0.0115
k_1	0.0002	0.0006	8.05E-05	0.0080
χ^2	0.0515	0.1454	0.2988	0.0092

Table 19: Statistical comparison between kinetic models

P_{AB}		$Mg_{0.81}Al$	$Mg_{1.38}Al$	$Mg_{1.82}Al$	$Mg_{2.93}Al$
A	B				
ER (Methanol adsorption)	LHHW (Methanol adsorption)	0.4773	7.0169	4.7893	1.0210
ER (Quasi steady state)	ER (Methanol adsorption)	1.2623	16.5059	0.2459	0.6784
ER (Methanol adsorption)	LHHW (surface reaction)	0.9129	0.3168	3.8518	0.2000
LHHW (Surface reaction)	LHHW (Methanol adsorption)	0.5229	22.1496	1.2434	5.1051
LHHW (Methanol adsorption)	ER (Quasi steady state)	1.6597	0.0086	0.8489	1.4437

Table 20: Properties of hyrotalcite catalysts[16]

Catalyst composition	Nominal Mg:Al ratio	Surface area (m^2/g)	Activity/mmolmin^{-1}.g(cat)$^{-1}$	Glyceryl Tributyrate Conversion %
$Mg_{0.81}Al$	1:1	166.4±8.3	0.004	42.4
$Mg_{1.38}Al$	2:1	121.9±6.1	0.01	49.2
$Mg_{1.82}Al$	3:1	92.5±4.6	0.024	55.3
$Mg_{2.93}Al$	4:1	104.1±5.2	0.025	74.8